ADVANCED MATERIALS TECHNOLOGIES
www.advmattechnol.de

Choice of Binder on Conversion Type CuO Nanoparticles toward Building High Energy Li-Ion Capacitors: An Approach Beyond Intercalation

*Manohar Akshay, Krishnan Subramanyan, Madhusoodhanan Lathika Divya, Yun-Sung Lee, and Vanchiappan Aravindan**

In this work, the assembly of lithium-ion capacitor (LIC) is described by pairing conversion type CuO nanoparticles recovered from the Cu current collector of spent lithium-ion batteries (r-CuO) as battery type electrode and activated carbon (AC) as the capacitor type electrode. The Li-storage property of r-CuO is studied in the presence of two binders (polyvinylidene fluoride, PVDF and carboxymethylcellulose, CMC) and found the aptness of CMC in comparison with PVDF. Accordingly, the Li/r-CuO half-cells with CMC binder exhibits better electrochemical performance such that even after 150 charge–discharge cycles, the cells could retain a specific capacity of ≈680 mAh g^{-1} at a current density of 0.2 A g^{-1}. The assembled LIC (AC/r-Cu^0+Li_2O) having electrochemically pre-lithiated r-CuO phase with balanced mass loading of AC can exhibit a maximum energy density of 65.6 Wh kg^{-1} with excellent cyclic stability at 2 A g^{-1} for 10,000 cycles with ≈80% capacity retention. It is worth mentioning that the thus fabricated LIC shows decent performance at high (50 °C) and low (–5 and 10 °C) temperature conditions.

1. Introduction

Excess use of fossil fuels leads to harmful effects such as climate change, global warming, exhaustible natural resources, and forcing research on eco-friendly energy production. As a result, there came the electric engine replacing conventional combustion engines. Present-day is the transition from traditional fossil fuels to radical renewable energy sources with an electrochemical way of storing them, which started with Sony's commercialization of the first Li-ion battery in 1991.[1] People diversified the energy storage devices with lithium-ion batteries (LIBs) and supercapacitors. Among these, particularly lithium-ion capacitors (LICs), seek much attention due to their eccentric behavior. Slow charge kinetics of batteries and low energy density of capacitors lead people to think of LIC. The LIC is the hybridization of high-power capacitors and high-energy batteries.[2,3] It generally comprises battery-type anode materials (with faradaic reaction) and activated carbon (AC) cathode (with the non-faradaic process), which brings a synergistic effect helping to advance along the diagonal of the Ragone plot. High power than LIBs and high energy than electrostatic double-layer capacitors (EDLCs) make it unique among other energy storage devices. Hence, applying LIC in public transport such as electric buses and trains has increased because of its ability to use the regeneration braking energy.[4,5]

The anode determines the overall performance of LIC, so researchers are focusing on these negative electrodes. Many studies have reported insertion type anodes[6,7] ($Li_4Ti_5O_{12}$, graphite, etc.), but the low energy density is the major limitation.[6] People now are more fascinated by conversion/alloying type materials (primarily metal oxides) because of their high theoretical capacity.[8–15] Nevertheless, volume variation and thereby cycling instability are the significant drawbacks of such anode. So, people attempt various composites to tackle these issues where intercalation and conversion/alloying reactions occur simultaneously.[16–18] The research attempts and reports on bare CuO as active anode material for LIC are not reported yet to the best of our knowledge. Hence, in this study, we chose CuO as anode for LIC assembly by considering its high theoretical capacity (674 mAh g^{-1}), chemical stability, abundance, and low cost. Further, due to the enormous demand for batteries, the number of spent LIBs is also increasing. Improper disposal of batteries may lead to air and water pollution. So, it became necessary to recycle the spent LIBs for environmental safety.[19–21] Hence, we used recovered CuO (r-CuO) as anode and the AC as the cathode in which faradaic reaction occurs in the former and non-faradaic reaction in the latter. We optimized the temperature and dwelling time of the r-CuO synthesis procedure and obtained the best electrochemical performance at 500 °C and 2 h of dwelling time. We also compared the electrochemical performance of r-Li/CuO

M. Akshay, K. Subramanyan, M. L. Divya, V. Aravindan
Department of Chemistry
Indian Institute of Science Education and Research (IISER)
Tirupati 517507, India
E-mail: aravind_van@yahoo.com
Y.-S. Lee
School of Chemical Engineering
Chonnam National University
Gwang-ju 61186, Republic of Korea

The ORCID identification number(s) for the author(s) of this article can be found under https://doi.org/10.1002/admt.202200423.

DOI: 10.1002/admt.202200423

half-cells assembled with two different binders: carboxymethyl cellulose (CMC) and polyvinylidene fluoride (PVDF). The commonly used PVDF binder has many demerits, such as low flexibility, harmful solvents such as *N*-methyl–2-pyrrolidinone (NMP), swelling at raised temperature, unsaturated > C=CF– bonds, thus resulting in a risk of thermal runaway of the cell, etc.[22–24] Also, the electrochemical performance of the CuO with PVDF binder was not much satisfying. Therefore, we used the water-soluble CMC binder for our entire electrochemical studies. The change in binder created a massive impact on the r-CuO vs. Li half-cell performance. Specific capacity and cyclic stability have increased significantly with just a difference in the binder. Thus, in this study, we introduce this environmentally friendly approach for assembling a new type of LIC, using r-CuO as active anode material and the water-soluble CMC as the binder, bringing green chemistry in the field of energy storage.

2. Results and Discussion

2.1. Characterization

The crystallographic structure, physical properties, and chemical composition of r-CuO were analyzed from powder X-ray diffraction (XRD) measurements, **Figure 1**a. The exhibited diffraction peaks are well-matched with JCPDS data (80-0076).[25–29] Sharp and prominent diffraction peaks at 35.52° and 38.7° corresponding to the $(11\bar{1})$ and (111) planes with interplanar space of 2.52 and 2.32 Å, respectively, and in good agreement with the crystalline monoclinic structure of CuO with the C12/c1(No.15) space group (a = 4.69 Å, b = 3.43 Å, and c = 5.14 Å). The average crystallite size was estimated based on the (111) peak using Debye Sherrer's formula ($D = 0.9\lambda/\beta \cos\theta$) and was obtained as ≈21 nm. Moreover, the absence of other peaks indicates the purity of r-CuO material obtained from spent LIBs. The X-ray photoelectron spectroscopy (XPS) survey scan includes peaks corresponding to Cu, O, and C and could provide information regarding the chemical composition at the surface of the material, Figure S1 (Supporting Information). The high-resolution XPS spectrum of Cu 2p consists of two main peaks and two satellite peaks. The peaks Cu $2p_{3/2}$ and Cu $2p_{1/2}$ can be deconvoluted into two peaks each, positioned at 933.19, 934.86 and 952.61, 954.04 eV, respectively corresponding to the Cu^{2+}/Cu^{0} group. The satellite peaks are generated due to the shake-up process when excess electrons are excited to higher energy states. The position of satellite peaks also indicates the 2^{+} oxidation state of Cu.[29–31] The O 1s spectrum can be deconvoluted into three components, centered at 529.51, 531.37, and 533.06 eV. The peak around 529.51 eV corresponds to O^{2-} ion in CuO, 531.37 eV links to oxygen vacancies in CuO lattice, and the peak at higher binding energy clearly indicates

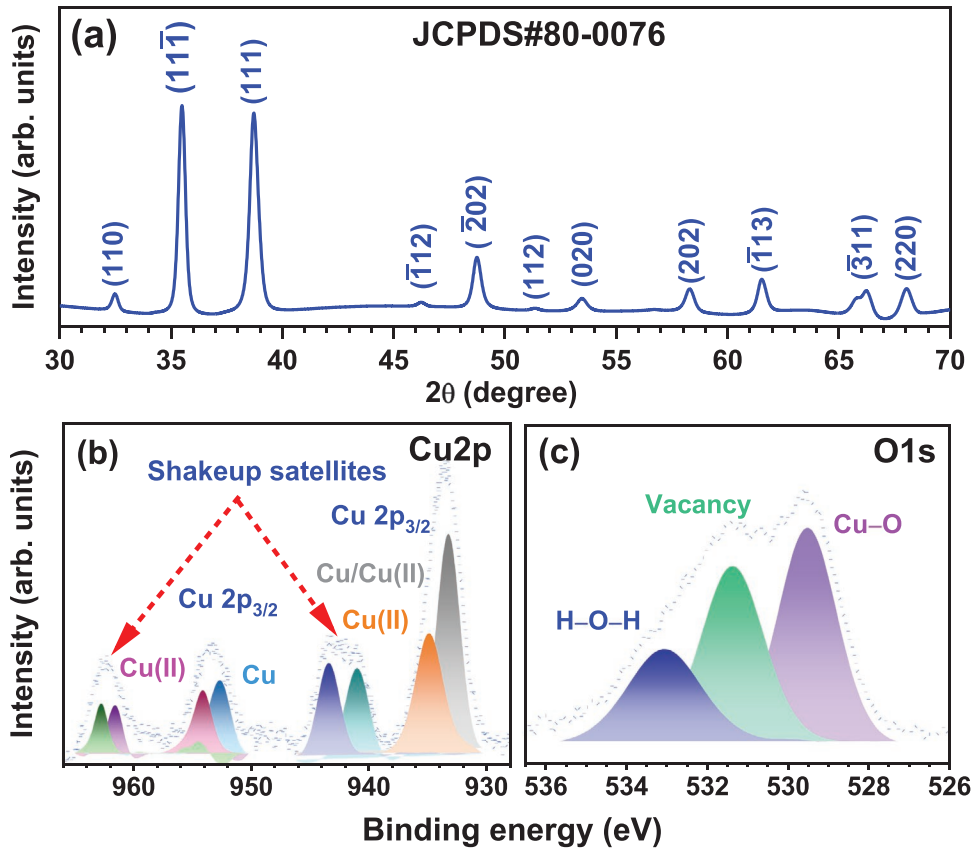

Figure 1. Physical characterization of r-CuO: a) X-ray diffraction (XRD) pattern, and b,c) high-resolution X-ray photoelectron spectroscopy (XPS) deconvolution spectra of Cu 2p and O 1s.

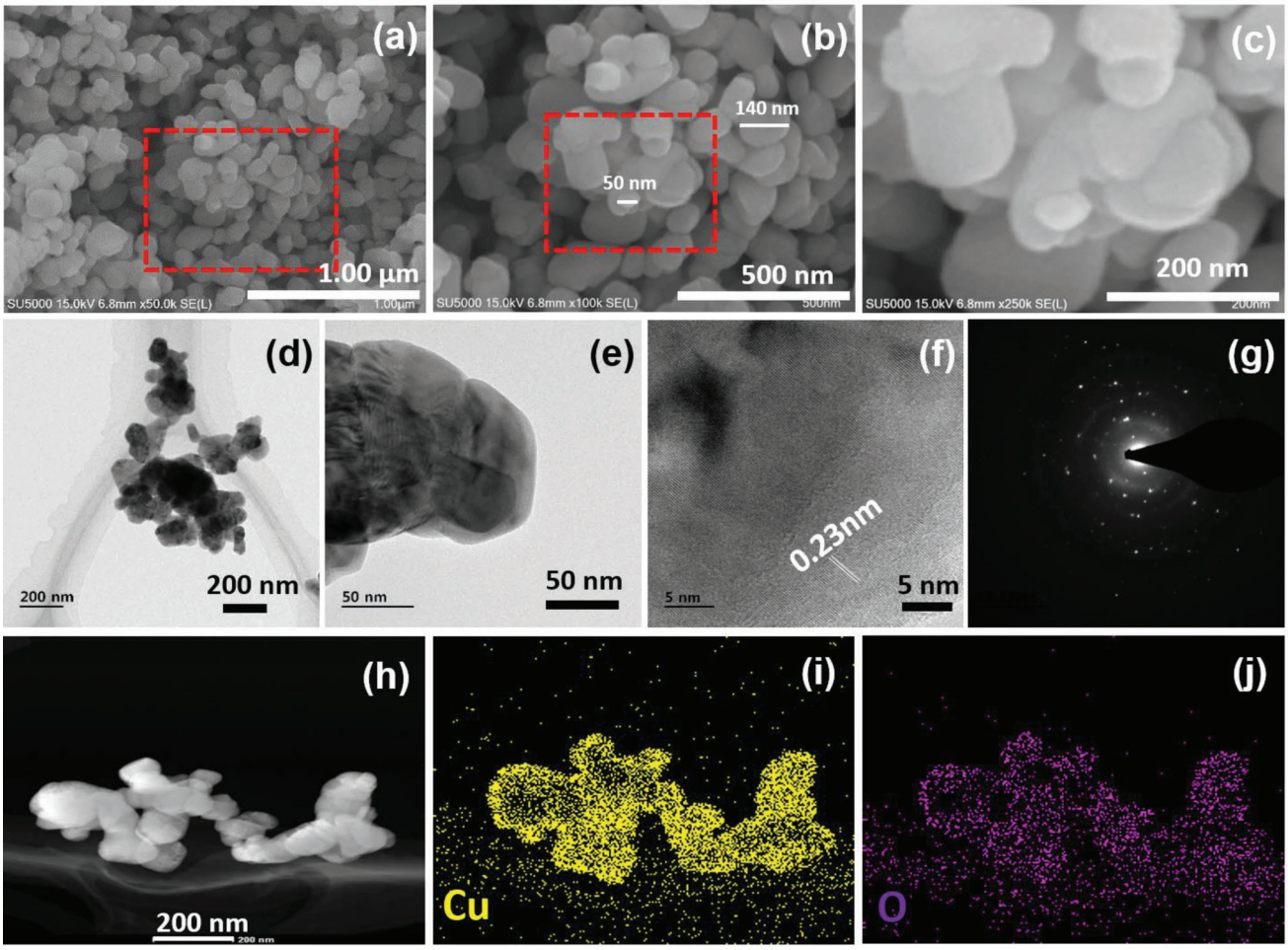

Figure 2. a–c) Field-emission scanning electron microscope (FE-SEM) images of r-CuO taken at different magnifications, d,e) transmission electron microscope (TEM) images at two different magnifications, f) high-resolution transmission electron microscope (HR-TEM) picture, g) selected area electron diffraction pattern (SAED) pattern, h) high angle annular dark-field imaging (HAADF) image, and i,j) energy-dispersive X-ray spectroscopy (EDS) elemental mapping.

the hydroxyl group.[32] The C 1s peak at 284 eV in the raw spectrum represents the C–C bond due to atmospheric contamination upon loading of the sample.

The particle size and morphology of r-CuO particles were studied from field-emission scanning electron microscope (FE-SEM) and transmission electron microscope (TEM) analysis. The FE-SEM images of different magnifications clearly show agglomeration of nanostructural spherical r-CuO particles with diameter ranges from 50 to 140 nm, **Figure 2**a–c. The size and morphology of r-CuO particles can be confirmed with TEM images, Figure 2d,e. High-resolution transmission electron microscope (HR-TEM) images clearly show lattice fringes with a spacing of 0.23 nm, which can be related to the (111) plane of r-CuO, Figure 2f. A series of diffraction rings with bright spots in the selected area electron diffraction pattern (SAED) indicates the polycrystalline nature of r-CuO particles Figure 2g. The STEM image recorded by the high angle annular dark-field imaging (HAADF) detector and Energy-dispersive X-ray spectroscopy (EDS) elemental mapping of r-CuO particles are displayed in Figure 2h–j. EDS images illustrate the elemental distribution of r-CuO particles.

2.2. Electrochemical Performance

The electrochemical performance was analyzed using Li metal as a reference and counter electrode in half-cell assembly. The galvanostatic charge–discharge (GCD) study was performed for Li/r-CuO half-cell in a potential window of 0.005 to 3 V vs. Li at the current density of 0.2 A g^{-1}. Initially, the electrochemical studies are performed with the conventional PVDF binder for the r-CuO electrode. GCD profile of Li/r-CuO half-cell using PVDF binder is shown in **Figure 3**. Apparently, the cycling stability of the Li/r-CuO half-cell was poor and specific capacity was reduced to 70 mAh g^{-1} within 75 cycles. Hence, we moved to a water-soluble environment friendly CMC binder. It provides better cyclic performance and mechanical stability to the volume variation due to conversion reaction.[14,23] Li/r-CuO half-cell using CMC binder delivered an initial discharge and charge capacity of ≈795 and ≈398 mAh g^{-1}, respectively, **Figure 4**. The irreversible capacity loss in the first discharge because of some irreversible electrochemical reactions resulting in the formation of the solid electrolyte interphase (SEI) layer.[11,33] However, it was found that the capacity increased with an

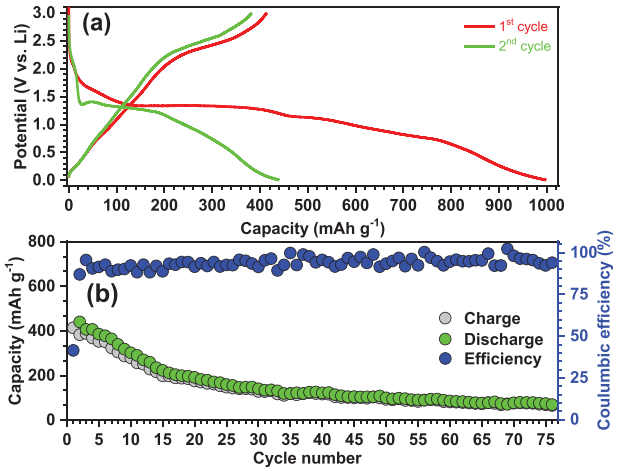

Figure 3. Electrochemical performance of Li/r-CuO half-cell using polyvinylidene fluoride (PVDF) binder at the current density of 0.2 A g^{-1}: a) Galvanostatic charge–discharge profile within the potential window of 0.005–3 V vs. Li, and b) cycling performance and corresponding Coulombic efficiencies (CEs).

increase in the cycle number and then stabilized. This is due to the further activation of the r-CuO electrode after each charge–discharge, which provides more electrochemical sites for activation.[12] After 75 cycles, cells with PVDF binder could retain only 16% of second discharge capacity (440 mAh g^{-1}) with Coulombic efficiency (CE) ≈94%. CMC-based cells could deliver ≈600 mAh g^{-1} with ≈100% CE, which is ≈154% higher than the second discharge capacity (389 mAh g^{-1}). Thus, CMC-based cells exhibited better cyclic stability and a specific capacity of ≈684 mAh g^{-1} after 150 cycles, which is far better than the PVDF binder. In the CMC binder, there are carboxylic groups that help in the formation of ester-like bonds between polymer molecules and active material, thereby forming a strong bond. This strong adhesion provides better cyclability and stability to the cell. Whereas in the case of PVDF binder, there is only

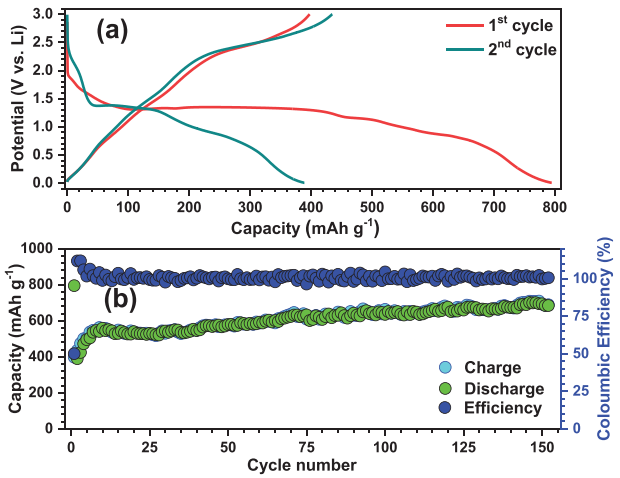

Figure 4. Electrochemical performance of Li/r-CuO half-cells using carboxymethyl cellulose (CMC) binder at the current density of 0.2 A g^{-1}: a) Galvanostatic charge–discharge profile within the potential window of 0.005–3 V vs. Li, and b) cycling performance and corresponding Coulombic efficiencies (CEs).

a very weak hydrogen bond between fluorine atom of binder and active material. Figure S2 (Supporting Information) shows the cyclic voltammetry (CV) profile of Li/r-CuO between 0.005 and 3 V vs. Li at a scan rate of 0.2 mV s^{-1}. The large current response noticed at ≈1.08 V vs. Li in the first cycle can be due to the decomposition of the structure and formation of the SEI layer. From the second cycle onwards, we could observe three reduction peaks around 2.13, 1.18, and 0.7 V vs. Li during discharge and three oxidation peaks around 1.4, 2.5, and 2.7 V vs. Li during charge, respectively. The reduction peak around 2.3 V vs. Li might be responsible for the partial reduction of r-CuO to $Cu^{II}_{1-x}Cu^{I}_{x}O_{1-x/2}$ solid solution phase ($0 \leq x \leq 0.4$)[34] and the reduction peaks at 1.18 and 0.7 V vs. Li might be attributed to subsequent formation of Cu_2O and Cu^0, respectively ($CuO + Li \rightarrow Cu^0 + Li_2O$).[35,36] The oxidation peak at 1.4 V vs. Li corresponds to the formation of Cu_2O, and peaks around 2.5 and 2.7 V vs. Li resulted in the formation of $Cu^{II}_{1-x}Cu^{I}_{x}O_{1-x/2}$ phase and the resultant creation of CuO phase ($Li_2O + Cu^0 \rightarrow CuO$).[37–39] Figure S3 (Supporting Information) displays the excellent rate performance and corresponding Coulombic efficiencies of Li/r-CuO half-cell. Electrochemical impedance spectroscopy (EIS) Nyquist plots (10 kHz to 1 Hz) before and after cycling of Li/r-CuO half-cells with both the binders are shown in Figure S4 (Supporting Information). Increased values of solution resistance and charge transfer resistance after cycling in the case of PVDF binder indicate instability of Li/r-CuO half-cell with PVDF binder. Whereas in the case of CMC binder, cycling induced a reduction in the value of resistances, pointing that such a system is more stable. In other words, the continuous growth of robust and resistive SEI layer tends to decline the capacity upon cycling for the case of PVDF based system. Parallelly, the positive electrode AC was also subjected to the half-cell studies at the current density of 0.2 A g^{-1} current rate in the 1.5 to 4.5 V vs. Li potential range. The Li/AC half-cell showed an initial discharge capacity of ≈102 mAh g^{-1} (Figure S5a, Supporting Information) and retained the specific capacity of ≈100 mAh g^{-1} even after 700 cycles (Figure S5b, Supporting Information). The AC/Li half-cell exhibited a pure non-faradaic process in which the Li^+ and PF_6^- ions get adsorbed and desorbed during the charge–discharge process. This non-faradaic nature of AC was also confirmed by the linear charge–discharge and rectangular CV profiles observed (Figure S6, Supporting Information).

In the case of the hybrid capacitor, the two electrodes have different energy storage mechanisms. The negative electrode is a battery-type electrode with faradaic behavior, and the positive electrode is a capacitor type with the non-faradaic mode of energy storage. Hence, mass balancing is significant during cell assembly and is given by the equation;

$$M_1C_1 = M_2C_2 \quad (1)$$

where M_1 is the mass of AC, M_2 is the mass of r-CuO, C_1 is the specific capacity of AC and C_2 is the specific capacity of r-CuO. The AC/r-Cu^0+Li_2O hybrid capacitor was fabricated by pairing pre-lithiated r-CuO is the anode with mass balanced AC cathode, in the presence of 1 M $LiPF_6$ in ethylene carbonate (EC):dimethyl carbonate (DMC) (1:1) electrolyte. For the electrochemical pre-lithiation process, Li/r-CuO half-cell was

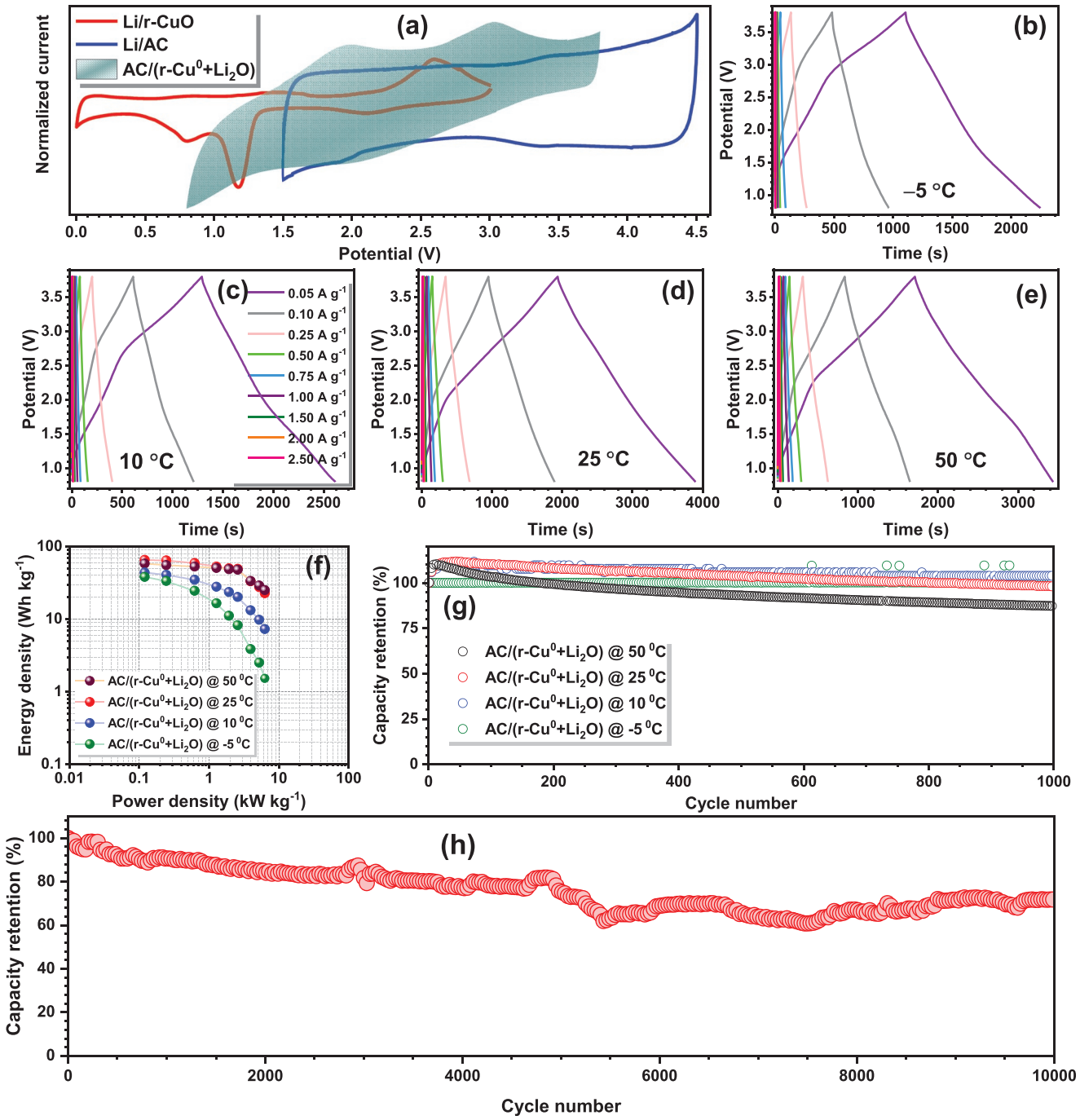

Figure 5. Electrochemical performance of AC/(r-Cu^0+Li_2O) lithium-ion capacitor (LIC): a) Typical cyclic voltammetry (CV) curves Li/r-CuO and Li/AC half cells and assembled LIC at a scan rate of 0.2 mV s^{-1}, b–e) the galvanostatic charge–discharge profile of LIC at different temperature conditions and at various current rates, f) the Ragone plot at varying temperature conditions, g) the cyclability of the LIC device at the corresponding temperature conditions for 1000 cycles, and h) the long-term cyclability of the device at ambient temperature conditions at the current density of 2 A g^{-1}.

fabricated and subjected to an initial discharge followed by two charge–discharge cycles. After the third discharge, the Li/r-Cu half-cell was dismantled, and the lithiated r-CuO electrode was coupled with the AC electrode. The AC electrode was made by balancing the mass by considering the third discharge capacity of the Li/r-CuO half-cell. The mass loading ratio of AC to r-CuO was taken to be ≈3.6 to balance the charge. **Figure 5** illustrates the electrochemical performance of LIC at ambient, low, and high-temperature conditions. Comparison of CV profiles of assembled LIC and the two half-cells recorded at a scan rate of 0.2 mV s^{-1} is depicted in Figure 5a. The typical CV profile of the LIC seems to be a hybridization of the CVs of both r-CuO and AC with a quasi-rectangular shape, which confirmed the hybrid behavior of the cell. In addition, it has been validated with

the three-electrode setup for the involvement of two different charge storage mechanisms in the LIC (Figure S7, Supporting Information). The fabricated LIC was subjected to GCD analysis at different current rates (0.1 to 2.5 A g^{-1}) in a 0.8 to 3.8 V potential window at different temperature conditions (–5, 10, 25, and 50 °C) to analyze the LIC operation at these environmental conditions (Figure 5b–e). The near-linear GCD profiles clearly indicate the involvement of different charge storage mechanisms in LIC. The assembled hybrid device delivered its best performance at room temperature. Figure 5f gives the Ragone plot obtained for the device at different temperature conditions, in which energy and power density values were calculated based on the total mass of active material present in the anode and cathode. The LIC could deliver the maximum energy density of 65.6 Wh kg^{-1} and power density of 6.3 kW kg^{-1} at 25 °C. While comparing with the lower temperatures (–5 °C and 10 °C), better energy density and power density were obtained at high temperatures (50 °C), which might be due to the increased electrolyte activity at the higher temperature.[7] This is the first work on the CuO-based electrodes for the LIC applications, and the values are compared with the state-of-the-art anode, graphite. The obtained values are lower than the conventional carbonaceous electrode-based systems (>100 Wh kg^{-1}) since the redox potential plays a vital role in determining the energy density of LIC.[40] Compared to the graphite (<0.1 V vs. Li), the redox event occurred for r-CuO at a potential of ≈0.7 V vs. Li, which eventually dilutes to attain a higher energy density. On the other hand, the LICs are known for their high current testing conditions; the higher redox potential of r-CuO certainly avoids the formation of Li-dendrites compared to graphite.[41] Therefore, the use of conversion type electrodes, i.e., CuO nanoparticles, is beneficial in terms of cell safety. Parallelly, most of the recycling attempts are performed to recover the active materials in both anode (graphite) and cathode (Li, Mn, Fe, Co, and Ni). Very rarely, the use of the current collector is reported irrespective of Al or Cu. The efficient and scalable conversion of Cu into CuO certainly paves the way to approach the 100% use of spent LIB components. Further studies are in progress to improve the energy density of the system without compromising the power capability. In addition, cyclability is another important factor, and the LIC was tested at various temperature conditions at a higher current density of 2 A g^{-1}. The cell performed well with high-capacity retention even after 1000 cycles with negligible fade in the retention (Figure 5g). The open-circuit voltage of the assembled LIC device was monitored concerning time, and it was found that the device exhibits a least self-discharge than conventional supercapacitor devices (Figure S8, Supporting Information).[42] Further, with the help of duplicate cells, long-term cyclability at ambient conditions was tested for 10 000 cycles at a current density of 2 A g^{-1}. At the end of 10 000 cycles, the LIC could retain ≈80% of the initial capacity. The retention of >80% capacity is highly significant for the potential use as an electrode in practical devices.

3. Conclusion

Our study consists of a simple, environmentally friendly, and economical method of synthesizing r-CuO from the anodic current collector of spent LIBs and using it as anode for LICs. We used a water-soluble CMC binder replacing conventional PVDF binder in electrode fabrication, thereby bringing green chemistry and better performance for Li/r-CuO half-cell. Our AC/r-Cu^0+Li_2O hybrid capacitor delivered a maximum energy and power density of 65.6 Wh kg^{-1} and 6.3 kW kg^{-1}. Temperature studies for different rates and long-term cycling were also performed to analyze the performance of cell at different climatic conditions. From the obtained results, it is concluded that the r-CuO is one of the best anode materials for LIC assembly in terms of safety and cyclability. The use of the passive component, Cu current collector, into the anode (CuO) active material clearly boosts the goal of achieving a circular economy in the recycling of spent LIBs.

4. Experimental Section

Recovery of Copper Foil from Spent LIB: The LIBs consist of graphite anode coated on copper foil current collector, various metal oxides, or phosphates as cathode coated on aluminum foil current collector, and polyolefin membrane as separators. These are wrapped in stainless-steel or aluminum metallic cases. For the recovery of copper foil, the spent mobile phone and laptop batteries were collected locally. To safely dismantle the collected spent batteries, the batteries were discharged by immersing them in NaCl solution overnight. The completely discharged batteries were sorted out by checking the open-circuit voltage using a multimeter. Then, it was washed with distilled water and dried in the hot air oven at 65 °C for 4 h. The batteries were then disassembled manually using cutters and pliers. First, the outer metallic case was removed, and the anode was separated from the cathode and separator. Cathode and separator were then individually stored for future use. The graphite was then removed from copper foil by submerging the anode in distilled water with sonication for an hour. It was then taken out and immersed in dimethylformamide (DMF, Sigma Aldrich, anhydrous, 99.8%) overnight to ensure complete dissolution of binder to separate all the graphite from foil and to obtain a clean foil. The foil was washed with distilled water, dried in the oven overnight, and stored in the dry box for future use. The graphite was collected by decanting the DMF and was stored.

Synthesis of r-CuO: The recovered copper foil was cut into small pieces, and 10 g of it was dissolved in a minimum nitric acid to get a copper nitrate ($Cu(NO_3)_2$) solution, which was then made up to 250 mL by slowly adding double-distilled water. Then 1 M NaOH solution was prepared and added to copper nitrate with constant stirring. This resulted in the precipitation of copper hydroxide ($Cu(OH)_2$). The NaOH was added continuously until the solution was slightly basic to ensure complete precipitation. The precipitate was allowed to settle down, and the supernatant was decanted out. The residue was washed with double distilled water until the pH dropped to 7. After the solution was neutralized, it was centrifuged for 5 min at 4000 rpm to filter out the $Cu(OH)_2$ precipitate. It was dried overnight in the oven at 65 °C and then powdered using mortar and pestle. Subsequently, it was calcined in the tube-furnace at 500 °C for 2 h at 5 °C min^{-1} ramp rate to obtain r-CuO nanoparticles, **Scheme 1**.

Material Characterization: Powder XRD was performed from angle 10° to 80° with a scan rate of 0.5° min^{-1} for the phase identification using Rigaku D/teX Ultra 250 diffractometer (40 kV, 200 mA, $\lambda = 1.5406$ Å) with Cu Kα radiation. Morphology and internal structure of CuO were analyzed using the FE-SEM S-4700 (Hitachi, Japan) and HR-TEM (TECNAI, Philips, the Netherlands, 200 keV), respectively. XPS (Multilab 2000, UK; monochromatic Al Kα radiation $h\nu$ = 1486.6 eV) examined the surface electronic states. HAADF detector and EDS were used to detect the elemental composition of r-CuO.

Cell Fabrication and Testing: Initially, the r-CuO and AC were tested in half-cell configuration using lithium metal as the counter/reference electrode. For the r-CuO electrode fabrication, the conventional slurry coating method was used. The slurry was prepared by mixing 80 wt%

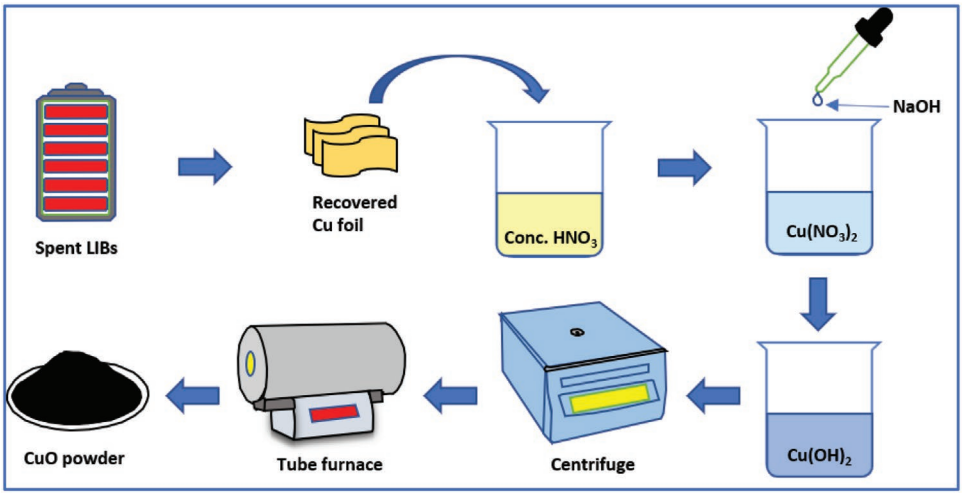

Scheme 1. Flowchart for the synthesis of CuO.

active materials (r-CuO), 10 wt% conductive carbons (acetylene black), and 10 wt% binders, either CMC or PVDF, in water or NMP as the solvent, respectively. It was kept for constant stirring overnight to obtain homogenous slurry. This homogenous slurry was coated on a copper foil using the doctor blade apparatus (MSK-AFA-III Automatic Thick Film Coater (MTI Corporation). It was dried in the hot air oven at 65 °C and then pressed in roll press (Tester Sangyo, Japan) to ensure uniform thickness for electrodes. The 14 mm electrodes were punched out using the hand-operated electrode cutter, and this was used as anode in cell fabrication. On the other hand, the positive electrode, commercial AC (YP 80F Kuraray, Japan; surface area: 2100 $m^2\ g^{-1}$, pore volume: 0.97 mL g^{-1}), was handmade using mortar and pestle. The AC, acetylene black (conductive carbon), and binder (teflonized acetylene black—TAB-2) were mixed in the ratio of 8:1:1 using ethanol solvent to form a uniform thin electrode layer. This thin electrode layer was pressed on a 16 mm stainless steel mesh current collector (Goodfellow, UK) and dried in the vacuum oven at 75 °C for at least a period of 4 h. Both these electrodes (r-CuO and AC) were subjected to half-cell and full-cell studies.

The half-cells and LICs were assembled using CR 2016 type coin cells in the Ar-filled glove box (MBRAUN, Germany) with H_2O level < 0.1 ppm and O_2 level < 0.1 ppm. The electrolyte used was 1 M $LiPF_6$ dissolved in EC and DMC in a 1:1 ratio (Tomiyama, Japan), and the separator was Whatman paper (1825-047, GF/F). The r-CuO and AC half-cells were fabricated with lithium metal counter/reference electrodes and tested for GCD in the potential range of 0.005 to 3 and 1.5 to 4.5 V vs. Li, respectively. The AC/r-Cu^0+Li_2O-based hybrid capacitor was fabricated such that the CuO half-cell was initially subjected to pre-lithiation (cell taken out after 3rd discharge) to introduce the Li^+ ions, followed by pairing with the AC electrode. Such that, initially, the r-CuO half-cell was discharged to 0.005 V vs. Li with a current rate of 200 mA g^{-1} followed by two charge–discharge cycles (0.005–3.00 V vs. Li), and then the cell was stopped. It was then dismantled and paired with a mass-balanced AC electrode to form an AC/r-CuO full-cell. The GCD experiment of both half-cells and LIC was carried out using the Biologic BCS 805 (France) battery tester. CV and EIS studies were carried out using an electrochemical workstation (Solartron, UK). The electrochemical performance of LIC at different temperatures was performed in an environmental chamber (Espec, Japan) in order to study the temperature-dependent performance of the assembled LIC.

Supporting Information

Supporting Information is available from the Wiley Online Library or from the author.

Acknowledgements

K.S. thanks the Department of Science and Technology (DST), Govt. of India, for the financial support through INSPIRE fellowship (IF180157). M.L.D. wishes to thank the funding through Women Scientist Scheme–B (DST/WOS–B/2018/2039) from the KIRAN division of the DST, Govt. of India. Y.S.L. acknowledges the financial support from the National Research Foundation of Korea (NRF) grant funded by the Korean government (Ministry of Science, ICT and Future Planning) (No. 2019R1A2C1007620). V.A. acknowledges the financial support from DST through Swarnajayanti Fellowship (DST/SJF/PSA-02/2019-20).

Conflict of Interest

The authors declare no conflict of interest.

Data Availability Statement

The data that support the findings of this study are available from the corresponding author upon reasonable request.

Keywords

Li-ion capacitor, binder, conversion, energy density, recycling

Received: March 15, 2022
Published online: May 12, 2022

[1] J. Hassoun, S. Panero, P. Reale, B. Scrosati, *Adv. Mater.* **2009**, *21*, 4807.
[2] M. Soltani, S. H. Beheshti, *J. Energy Storage* **2021**, *34*, 102019.
[3] A. Jagadale, X. Zhou, R. Xiong, D. P. Dubal, J. Xu, S. Yang, *Energy Storage Mater.* **2019**, *19*, 314.
[4] D. P. Dubal, O. Ayyad, V. Ruiz, P. Gómez-Romero, *Chem. Soc. Rev.* **2015**, *44*, 1777.
[5] J. Ding, W. Hu, E. Paek, D. Mitlin, *Chem. Rev.* **2018**, *118*, 6457.
[6] V. Aravindan, J. Gnanaraj, Y.-S. Lee, S. Madhavi, *Chem. Rev.* **2014**, *114*, 11619.

[7] M. L. Divya, S. Natarajan, Y.-S. Lee, V. Aravindan, *J. Mater. Chem. A* **2020**, *8*, 4950.
[8] M. V. Reddy, G. V. Subba Rao, B. V. R. Chowdari, *Chem. Rev.* **2013**, *113*, 5364.
[9] V. Aravindan, Y.-S. Lee, *J. Phys. Chem. Lett.* **2018**, *9*, 3946.
[10] K. Cao, T. Jin, L. Yang, L. Jiao, *Mater. Chem. Front.* **2017**, *1*, 2213.
[11] F. Klein, R. Pinedo, B. B. Berkes, J. Janek, P. Adelhelm, *J. Phys. Chem. C* **2017**, *121*, 8679.
[12] Y. Xu, K. Chu, Z. Li, S. Xu, G. Yao, P. Niu, F. Zheng, *Dalton Trans.* **2020**, *49*, 11597.
[13] H. Liu, Y. Lin, Z. Hu, R. Hu, H. Ruan, L. Zhang, *J. Nanomater.* **2016**, *2016*, 2864962.
[14] L. Wang, K. Tang, M. Zhang, X. Zhang, J. Xu, *Funct. Mater. Lett.* **2014**, *07*, 1440008.
[15] Y. Lu, L. Yu, X. W. Lou, *Chem* **2018**, *4*, 972.
[16] S.-H. Lee, G. Yoo, J. Cho, S. Ryu, Y. S. Kim, J. Yoo, *J. Alloys Compd.* **2020**, *829*, 154566.
[17] J. Zhang, B. Wang, J. Zhou, R. Xia, Y. Chu, J. Huang, *Materials* **2017**, *10*, 72.
[18] M. L. Divya, S. Praneetha, Y.-S. Lee, V. Aravindan, *Composites, Part B* **2022**, *230*, 109487.
[19] S. Natarajan, D. S. Lakshmi, H. Bajaj, D. Srivastava, *J. Environ. Chem. Eng.* **2015**, 2538.
[20] D. L. Thompson, J. M. Hartley, S. M. Lambert, M. Shiref, G. D. J. Harper, E. Kendrick, P. Anderson, K. S. Ryder, L. Gaines, A. P. Abbott, *Green Chem.* **2020**, *22*, 7585.
[21] S. Natarajan, M. Akshay, V. Aravindan, *Adv. Sustainable Syst.* **2022**, *6*, 2100432.
[22] J. Ming, H. Ming, W.-J. Kwak, C. Shin, J. Zheng, Y.-K. Sun, *Chem. Commun.* **2014**, *50*, 13307.
[23] R. Wang, L. Feng, W. Yang, Y. Zhang, Y. Zhang, W. Bai, B. Liu, W. Zhang, Y. Chuan, Z. Zheng, H. Guan, *Nanoscale Res. Lett.* **2017**, *12*, 575.
[24] S. S. Zhang, K. Xu, T. R. Jow, *J. Power Sources* **2004**, *138*, 226.
[25] Y.-K. Hsu, Y.-C. Chen, Y.-G. Lin, *Appl. Surf. Sci.* **2015**, *354*, 85.
[26] S. M. Sathiya, G. S. Okram, M. Jothi, *Adv. Mater. Proc.* **2017**, *2*, 371.
[27] D. Manyasree, K. M. Peddi, R. Ravikumar, *Int. J. Appl. Pharmaceut.* **2017**, *9*, 71.
[28] D. Zhu, L. Wang, W. Yu, H. Xie, *Sci. Rep.* **2018**, *8*, 5282.
[29] H. Siddiqui, M. R. Parra, P. Pandey, M. S. Qureshi, F. Z. Haque, *J. Sci.: Adv. Mater. Devices* **2020**, *5*, 104.
[30] D. Svintsitskiy, C. Alexei, E. Slavinskaya, O. Stonkus, A. Stadnichenko, S. Koscheev, A. Boronin, *J. Mol. Catal. A: Chem.* **2012**, *368–369*, 95.
[31] X. Wang, B. Zhang, W. Zhang, M. Yu, L. Cui, X. Cao, J. Liu, *Sci. Rep.* **2017**, *7*, 1584.
[32] J. Jiang, X. X. Liu, J. Han, K. Hu, J. S. Chen, *Processes* **2021**, *9*, 680.
[33] T. Zhang, Z. Mao, X. Shi, J. Jin, B. He, R. Wang, Y. Gong, H. Wang, *Energy Environ. Sci.* **2022**, *15*, 158.
[34] W. Yuan, J. Luo, B. Pan, Z. Qiu, S. Huang, Y. Tang, *Electrochim. Acta* **2017**, *241*, 261.
[35] V. Aravindan, Y.-S. Lee, S. Madhavi, *Adv. Energy Mater.* **2015**, *5*, 1402225.
[36] R. Sahay, P. Suresh Kumar, V. Aravindan, J. Sundaramurthy, W. Chui Ling, S. G. Mhaisalkar, S. Ramakrishna, S. Madhavi, *J. Phys. Chem. C* **2012**, *116*, 18087.
[37] S. J. Hibble, C. Malitesta, P. G. Dickens, *Solid State Ionics* **1990**, *39*, 289.
[38] W. Chen, H. Zhang, Z. Ma, B. Yang, Z. Li, *J. Mater. Chem. A* **2015**, *3*, 14202.
[39] Z. Deng, Z. Ma, Y. Li, Y. Li, L. Chen, X. Yang, H.-E. Wang, B.-L. Su, *Front. Chem.* **2018**, *6*, 428.
[40] S. Natarajan, Y.-S. Lee, V. Aravindan, *Chem. - Asian J.* **2019**, *14*, 936.
[41] P. Sennu, S. Madhavi, V. Aravindan, Y.-S. Lee, *ACS Nano* **2020**, *14*, 10648.
[42] Z. Mao, H. Wang, D. Chao, R. Wang, B. He, Y. Gong, H. J. Fan, *Small* **2020**, *16*, 2001950.